BIOCHEMISTRY
including biophysical chemistry & molecular biology
Article

Biochemistry **2010,** *49,* 4779–4785 4779
DOI: 10.1021/bi902190r

The Human Estrogen Sulfotransferase: A Half-Site Reactive Enzyme[†]

Meihao Sun[‡] and Thomas S. Leyh*

Microbiology and Immunology, Albert Einstein College of Medicine, 1300 Morris Park Avenue, Bronx, New York 10461-1926
[‡]Present address: College of Chemistry and Life Sciences, Zhejiang Normal University, 688 Yingbin Blvd., Jinhua, Zhejiang, China 321004.

Received December 21, 2009; Revised Manuscript Received April 29, 2010

ABSTRACT: The affinity of 17β-estradiol (E_2) for the estrogen receptor is weakened beyond the point of physiological relevance by the transfer of the sulfuryl moiety ($-SO_3$) from PAPS (3′-phosphoadenosine 5′-phosphosulfate) to the 3′-hydroxyl of E_2. The mechanism of this transfer reaction, catalyzed by estrogen sulfotransferase (EST), is investigated here in detail. The enzyme (a dimer of identical protomers) presents a clear example of half-sites reactivity—only one of the subunits of the dimer produces product during the catalytic cycle. This is the first example of half-sites reactivity in the sulfotransferase family. A burst of product, with an amplitude that corresponds to one-half of the available active sites, reveals that the mechanism is rate-limited by product release. The equilibrium constant governing interconversion of the substrate ($E\cdot PAPS\cdot E_2$) and product ($E\cdot PAP\cdot E_2S$) central complexes was determined and is strongly biased toward product ($K_{eq\ int} \sim 49$). Slow product release allows the interconversion of the central complexes to approach equilibrium, with the result that $K_{eq\ int}$ becomes nearly linearly coupled to K_m and contributes a factor of ~30 to the steady-state affinity of the enzyme for substrate. Typical of its family, estrogen sulfotransferase is partially k_{cat}-inhibited by its acceptor substrate, E_2. This inhibition does not influence the burst kinetics and thus occurs after formation of the product central complex, a finding consistent with the slow escape of PAP from the nonreactive $E\cdot PAP\cdot E_2$ complex.

Estrogen sulfotransferase (EC 2.8.2.4) catalyzes transfer of the sulfuryl moiety (SO_3) from PAPS (3′-phosphoadenosine 5′-phosphosulfate) to the 3′-hydroxyl of 17β-estradiol (E_2) (reaction 1).

$$E_2 + PAPS^{4-} \rightleftarrows E_2S^- + PAP^{4-} + H^+ \quad (1)$$

The remarkably large chemical potential of the phosphoric–sulfuric acid anhydride bond found in PAPS [$\Delta G_{hydrolysis}^{o\prime} = -19$ kcal/mol (*1*, *2*)] contributes to the favorable energetics of the transfer reaction [K_{eq} = 4200 (*3*)]. Initial rate and ligand binding studies indicate the catalysis occurs via a random bi-bi mechanism (*3*). Chemical cross-linking and mutagenesis studies have shown that EST, like most cytosolic sulfotransferaes, is a dimer whose monomers are linked by a small interface found in each of the 17 sulfotransferase crystal forms available in the Protein Data Bank (PDB) (*4*–*6*).

Sulfation of E_2 prevents it from binding to the estrogen receptor (*7*), and hydrolytic cleavage of the sulfuryl group from E_2S [catalyzed by sulfatases (*8*, *9*)] regenerates the receptor-active form of the hormone. The balance of these activities is expected to determine the receptor binding potential of the estrogen pool in living cells. Similar sulfation–desulfation cycles regulate numerous other metabolites and processes, including steroid hormones (*10*, *11*), signaling peptides (*12*–*15*), heparin (*16*, *17*), hemostasis (*18*–*20*), lymph circulation (*21*), and numerous drugs and xenobiotics (*22*, *23*).

The human estrogen sulfotransferase (EST), the focus of this work, is one of approximately 10 human cytosolic sulfotransferases (*24*, *25*), many of which exhibit distinct spatiotemporal distributions at the organismal level (*26*). The typically broad substrate specificities of these isoforms are likewise distinct (yet often overlapping), and together, they comprise a robust sulfation network whose proper functioning is critical to the well-being of the individual. The cellular levels of EST have been causally linked to the estrogen growth response of cell lines derived from estrogen-dependent breast and endometrial tumors. While present in normal control cells, EST is not detected in most estrogen growth-dependent cancer cell lines (*27*), and expression of EST at wild-type levels in these otherwise EST-depleted cells abrogates the responses normally associated with E_2 activation, including the E_2 growth response (*28*, *29*).

In this work, the rates and equilibria of several of the reactions that occur on the surface of EST during its catalytic cycle have been defined. In the process, it was discovered that the enzyme (a dimer of identical subunits) is half-site reactive; that is, only one of the subunits produces product during a given catalytic cycle. Furthermore, the mechanism is such that the ratio of the central complexes in the steady state is linearly coupled to K_m and enhances the affinity of EST for its substrates ~30-fold, suggesting that selective stabilization of the central complexes may contribute significantly to substrate selection within the family. Finally, we demonstrate that the partial substrate inhibition that is characteristic of sulfotransferases becomes operative in the mechanism subsequent to formation of enzyme-bound product, suggesting that inhibition operates by slowing the release of product.

[†]Supported by National Institutes of Health Grant GM54469.
*To whom correspondence should be addressed: The Department of Microbiology and Immunology, Albert Einstein College of Medicine, 1300 Morris Park Ave., Bronx, NY 10461-1926. Phone: (718) 430-2857. Fax: (718) 430-8711. E-mail: leyh@aecom.yu.edu.

Published on Web 04/29/2010

MATERIALS AND METHODS

Materials. The enzymes, reagents, and salts, unless specified otherwise, were of the highest grades available from Sigma-Aldrich Co. Estradiol was purchased from Steraloids Inc. Radiolabeled estradiol [[2,4,6,7-^{3}H]estradiol (90 Ci/mmol)] was purchased from NEN Life Science Products. [^{35}S]SO_4 was obtained from ICN Pharmaceuticals. PAPS was purchased from S. Singer (University of Dayton, Dayton, OH). Factor Xa protease was purchased from Enzyme Research Laboratories. The Bradford assay mix was obtained from Bio-Rad. Amylose resin was purchased from New England Biolabs Inc. Q Sepharose Fast Flow and Superdex 200 resins were purchased from Amersham Pharmacia Biotech. Poly(ethylenimine) cellulose-F thin-layer chromatography (PEI-F TLC)[1] sheets were purchased from EM Science. Centricon concentrators (10 kDa cutoff) were obtained from Millipore.

Purification and Quantitation of Estrogen Sulfotransferase. The purification protocol was described previously (*3*). The >95% pure enzyme (A_{280} = 1.7) was aliquoted, rapidly frozen in a dry ice/EtOH bath, and stored at −70 °C in buffer containing 50 mM KPO_4 (pH 6.3) and glycerol (10%, v/v). The EST concentration was determined optically at λ_{280} using the following gravimetrically determined extinction coefficient (*3*) (ε_{280}* = 1.7 ± 0.1 A_{280} mL mg^{-1} cm^{-1}). The gravimetrically determined extinction coefficient was corroborated by determining the extinction coefficient in 6.0 M guanidinium chloride (*30*) (ε_{280}* = 1.6 ± 0.08 A_{280} mL mg^{-1} cm^{-1}). The gravimetrically determined value is used throughout this work.

[^{35}*S*]*PAPS Synthesis*. [^{35}S]PAPS was synthesized in a 0.50 mL reaction mixture that contained the following: sulfate activating complex (*Rhodobacter sphaeroides*), 0.050 unit/mL [note this complex exhibits both ATP sulfurylase and APS kinase activity (*31*), and unit is quoted for conversion of ATP and SO_4 to PAPS]; inorganic pyrophosphatase (baker's yeast), 0.10 unit/mL; pyruvate kinase (rabbit muscle), 0.17 unit/mL; [^{35}S]SO_4 (1.0 mCi, 1491 Ci/mmol); ATP (6.0 mM); PEP (2.0 mM); $MgCl_2$ (8.0 mM); KCl (100 mM); and Hepes (50 mM, pH 8.0). The reaction was quenched after 5hr by addition of EDTA to 10 mM, and protein was then removed by filtration (Centricon 10). [^{35}S]PAPS was purified chromatographically by anion exchange HPLC (AX300, SynChropak) using an isocratic eluant ($NaPO_4$, 0.30 M, pH 6.4). The purified [^{35}S]PAPS was desalted and concentrated to dryness as described previously (*32*). The compound was dissolved in Hepes (50 mM, pH 8.0) and stored at −70 °C.

Quenched-Flow Studies of the EST-Catalyzed Reaction. Reactions were initiated and quenched using a KinTek quench-flow instrument (model RQF-3). The compositions of the reaction and quench solutions are defined in the figure legends. Following quenching, the samples were centrifuged to remove denatured enzyme, and the pH of the supernatant was adjusted to 9.0 by addition of 1.0 M Tris (pH 9.0). E_2 was extracted from the aqueous phase twice, using CCl_4, and E_2S was quantitated by liquid scintillation counting (Wallac 1409DSA). Total counts were corrected slightly (<10%) by subtraction of residual aqueous [^{3}H]E_2 E2 counts that were determined in control experiments from which EST was omitted.

Simulating the Ligand Distribution Experiment. [E·E_2S] versus [EST] was simulated for half-site and full-site models using Gepasi (3.21) (*33*). The simulation model allowed the enzyme to bind one E_2 per active site and used a K_d of 26 nM (*3*). The singly (E·E_2) and doubly (E·E_2·E_2) occupied dimer concentrations were calculated, and these values were used to calculate product formed after 0.30 s by assuming either that 50% of all of the bound E_2 is converted to product [i.e., the full-site model with $K_{eq\ int}$ = 1.0] or that 98% of [E·E_2] + 0.50[E·E_2·E_2] is converted to product (i.e., the half-site model with $K_{eq\ int}$ = 49).

Classical Trapping of [^{35}*S*]*PAPS*. A pulse solution containing EST (1.0 μM) (active sites) and [^{35}S]PAPS (1.5 μM) was mixed with a chase solution of equal volume containing E_2 (3.6 μM) and unlabeled PAPS (2.7 mM). Five seconds later, the reaction was quenched by addition of an equal volume of NaOH to a final concentration of 0.30 M. The quenched solutions were then heated in a boiling water bath for 1.0 min and spun to remove the precipitate. The deproteinized supernatant was neutralized by addition of MES (1.0 M, pH 6.3) to a final concentration of 0.50 M. [^{35}S]E_2S and [^{35}S]PAPS were then separated on PEI-F TLC plates using a LiCl (0.9 M) mobile phase and quantitated as described previously (*34*). The pulse and chase solutions were equilibrated at 23 ± 2 °C prior to mixing and contained KPO_4 (50 mM, pH 6.3), glycerol (10%, v/v), $MgCl_2$ (7.0 mM), and DTT (1.0 mM).

Pre-Steady-State Trapping of [^{35}*S*]*PAPS*. A solution containing EST (1.0 μM, active sites) was mixed rapidly (using a KinTek quench flow) with a solution of equal volume that was identical except that it lacked EST and contained E_2 and [^{35}S]PAPS (3.6 and 4.5 μM, respectively). The reaction was allowed to proceed for 0.30 s before the solution was mixed rapidly with an equal volume of chase solution containing 2.3 mM PAPS and 1.8 μM E_2. The reaction was quenched 30 s after the addition of chase by addition of NaOH (0.66 M) to a final concentration of 0.33 M. The separation and quantitation of E_2S were the same as described above. Control experiments quenched immediately after the reaction proceeded for 0.3 s were run to determine the amount of E_2S formed at the moment of the chase addition. Solutions were equilibrated at 25 ± 2 °C prior to mixing and contained KPO_4 (50 mM, pH 6.3), glycerol (10%, v/v), $MgCl_2$ (7.0 mM), and DTT (1.0 mM).

RESULTS AND DISCUSSION

A Pre-Steady-State Burst of Product Formation. To identify and characterize rate-determining step(s) in the EST mechanism, pre-steady-state quenched-flow experiments were performed in the forward (E_2S-forming) direction. Enzyme (1.0 μM) saturated with E_2 [3.6 μM, 280K_i (*34*)] was mixed rapidly with an equal volume of a solution containing a saturating concentration of PAPS (18.0 μM, 305K_m), and reactions were quenched on a time scale that spanned the pre-steady-state and early steady-state regions of the catalytic cycle (Figure 1). The burst of product that was observed showed no signs of a lag and was followed by linear steady-state turnover. Virtually all of the E_2 was converted to E_2S at the end point of the reaction (not shown). A burst is indicative of a rate-determining step(s) in the product-release branch of the catalytic cycle. Such a step might occur at the point of delivery of product into solution or be associated with isomerization before or after product release. A striking feature of the burst is that its amplitude corresponds to precisely one-half of an enzyme active site equivalent, suggesting

[1]Abbreviations: Hepes, 4-(2-hydroxyethyl)-1-piperazineethanesulfonic acid; MES, 2-(*N*-morpholino)ethanesulfonic acid; PEI-F TLC, poly(ethylenimine) cellulose-F thin-layer chromatography; PEP, phosphoenolpyruvate; unit, micromoles of substrate converted to product per minute at V_{max}.

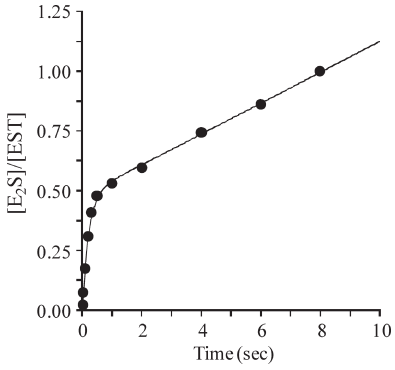

FIGURE 1: Burst of E_2S formation. We initiated E_2S synthesis by rapidly mixing a solution containing EST (1.0 μM, dimer), [^{3}H]E_2 (3.6 μM, 720K_m, specific activity of 90 Ci/mmol), glycerol (10%, v/v), $MgCl_2$ (7.0 mM), DTT (1.0 mM), and 50 mM KPO_4 (pH 6.3) with a solution of equal volume that was identical except that it lacked EST and E_2 and contained PAPS (18.0 μM, 305K_m). We quenched the reactions by rapidly mixing the reacting solutions with an equal volume of HCl (0.66 M). [^{3}H]E_2 was extracted from the quenched mixture using CCl_4, and [^{3}H]E_2S, which remained in the aqueous phase, was counted (see Materials and Methods). All solutions were equilibrated at 25 ± 2 °C prior to being mixed. Reactions were performed in triplicate and averaged. The smooth curve represents the best fit of the averaged data to the expression $A_0(1 - e^{-\lambda t}) + k_{cat}t$.

either that EST is a half-sites reactive enzyme or that the ratio of substrate-bound to product-bound forms of the enzyme during steady-state turnover is approximately 1.

A general model for an enzymatic burst is given by eq 2 (*35*, *36*)

$$[\text{product}]/[\text{enzyme}] = A_0(1 - e^{-\lambda t}) + k_{cat}t \qquad (2)$$

which sums the exponential and linear phases of the reaction. When eq 2 is fit to the EST burst data using a nonlinear least-squares algorithm, the following best-fit parameters are obtained: $A_0 = 0.52 \pm 0.02$, $\lambda = 4.2 \pm 0.4\ s^{-1}$, and $k_{cat} = 0.036 \pm 0.004\ s^{-1}$. The progress curve predicted by these parameters is represented by the solid line passing through the data in Figure 1. Equation 2 assumes that both active sites in the dimer are capable of turning over. If, instead, the enzyme is half-sites reactive, the best-fit k_{cat} increases by a factor of 2, to $0.072 \pm 0.004\ s^{-1}$. The value of the amplitude (A_0), 0.52, reiterates the possibility that only half of the EST active sites may be capable of turning over.

Mechanism I is perhaps the simplest mechanism capable of predicting burst of product that is stoichiometric with enzyme. The mechanism assumes that substrate binding is fast relative to E·P complex formation and aggregates all of the rate constants governing product release into a single net-rate constant, k_3.

$$E\cdot S \underset{k_2}{\overset{k_1}{\rightleftarrows}} E\cdot P \xrightarrow{k_3} E + P \qquad (I)$$

Utilizing mechanism I, product formation is again given by eq 2 (*35*, *36*):

$$\lambda = k_1 + k_2 + k_3$$

$$A_0 = k_1(k_1 + k_2)/(k_1 + k_2 + k_3)^2$$

$$k_{cat} = k_1k_3/(k_1 + k_2 + k_3)$$

The best-fit constants (k_1, k_2, and k_3) obtained using this form of eq 2 depend on whether the values of $[E_2S]/[E]_{tot}$ are calculated using monomer or dimer concentrations of EST. Normalizing to the monomer tacitly assumes that both subunits of a fully occupied dimer are capable of turning over and produces best-fit constants that predict an internal equilibrium constant ($K_{eq\ int} = [EP]/[ES] = k_1/k_2$) that is near unity: $k_1 = 2.2 \pm 0.2$, $k_2 = 1.8 \pm 0.2\ s^{-1}$, and $k_3 = 0.071 \pm 0.009\ s^{-1}$. On the other hand, normalizing to the dimer assumes half-site reactivity and yields a $K_{eq\ int}$ that strongly favors E·P complex formation: $k_1 = 4.4 \pm 0.3$, $k_2 \sim 0\ s^{-1}$, and $k_3 = 0.071 \pm 0.009\ s^{-1}$.

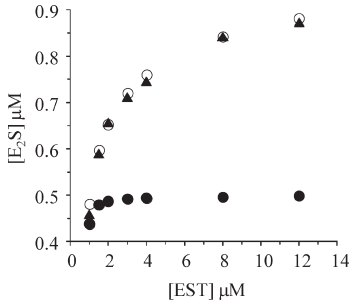

FIGURE 2: Confirmation of half-sites reactivity. We initiated the reactions by mixing a solution containing PAPS (16 μM), glycerol (10%, v/v), $MgCl_2$ (7.0 mM), DTT (1.0 mM), and 50 mM KPO_4 (pH 6.3) with an equal volume of an identical solution that did not contain PAPS but did contain [^{3}H]E_2 (2 μM) and various concentrations of EST (2.0, 3.0, 4.0, 6.0, 8.0, 16.0, and 24.0 μM, monomer concentrations). The plotted E_2S concentrations represent the E_2S formed in reactions quenched at 0.30 s; at this time point, the burst is essentially complete and steady-state turnover contributes only slightly to overall product formation (see Figure 1). Triangles (▲) represent experimentally determined E_2S concentrations]. Empty circles (○) represent E_2S concentrations predicted using a half-site reactivity model in which $K_{eq\ int} \gg 1.0$. Filled circles (●) represent E_2S concentrations predicted using a full-site reactivity model in which $K_{eq\ int} \sim 1.0$. The simulations are described in Materials and Methods. Quenching and quantitation were as described in the legend of Figure 1 (also, see Materials and Methods). Experimental values were determined in triplicate and averaged. All solutions were equilibrated at 25 ± 2 °C prior to being mixed.

Confirming the Half-Site Mechanism. The amplitude of the burst shown in Figure 1 (0.52) represents a stoichiometry ([product formed]/[saturated subunits]) obtained under conditions where both of the dimer subunits are saturated. Given this amplitude and condition, we can conclude that for a full-site mechanism (identical subunits) each subunit spends approximately equal time in substrate and product forms during turnover or, for a half-site mechanism, that the single dimer subunit that turns over spends the majority of its time in product complexes. These models predict that under conditions where only one of the dimer subunits is bound to substrate, the amplitude for the half-site mechanism will be twice that of the full-site mechanism.

Capitalizing on these differences to identify the operative mechanism, we determined the amplitude at fixed [^{3}H]E_2 and PAPS concentrations [1.0 μM (K_m = 5.0 nM) and 8.0 μM (K_m = 59 nM), respectively] over a range of EST concentrations (1−12 μM) chosen such that E_2 remains virtually entirely enzyme-bound throughout the titration (Figure 2). At the lowest EST concentration, both of the dimer subunits are saturated, and either model predicts an amplitude of ~0.5. In contrast, at the highest EST concentration (12 μM), the models make very different predictions with regard to amplitude: the full-site model continues to predict an amplitude of ~0.5, whereas the half-site model predicts an amplitude of 0.88 at 12 μM EST due to the fact that the majority of the dimers will have only one active site occupied (see Simulating the Ligand Distribution Experiment). The titration demonstrates that as the EST concentration begins

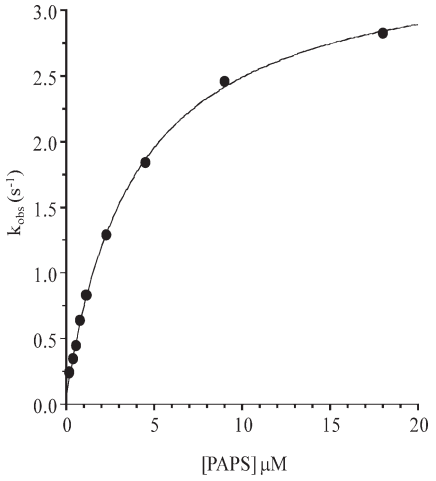

FIGURE 3: k_{obs} vs [PAPS] for E_2S synthesis. We initiated the reactions by rapidly mixing a solution containing EST (1.0 μM), [^{3}H]E_2 (3.6 μM, specific activity of 90 Ci/mmol), glycerol (10%, v/v), $MgCl_2$ (7.0 mM), DTT (1.0 mM), and 50 mM KPO_4 (pH 6.3) with an equal volume of an identical solution that did not contain EST and E_2 but did contain various concentrations of PAPS (0.375, 0.75, 1.125, 1.5, 2.25, 4.5, 9, 18, and 36 μM). Quenching and quantitation of product are described in the legend of Figure 1 (also, see Materials and Methods). All solutions were equilibrated at 25 ± 2 °C prior to being mixed. Reaction rates at each PAPS concentration were obtained from least-squares regressions of triplicate, averaged four-point progress curves taken during the first 15% of product formation. We obtained k_{obs} values by dividing the reaction rate by the enzyme concentration (0.50 μM). The solid line represents behavior predicted by the best fit of a two-step model that includes PAPS binding and interconversion of the central complexes (see Results and Discussion).

to exceed that of E_2, causing the ligand to redistribute such that the fraction of dimers having only one subunit bound to E_2 increases, the amplitude increases in a well-behaved fashion to 0.88, and the data trend suggests a yet larger amplitude at EST concentrations >12 μM (Figure 2). The simulated amplitudes for the half-site (○) and full-site models (●) strongly favor the half-site mechanism (see Materials and Methods). Thus, EST appears to be a half-site reactive enzyme.

Internal Equilibrium Constant ($K_{eq\ int}$). Fitting the burst with a half-site model suggested that the central complex equilibrium constant favors product and revealed that k_2 (mechanism I) is too small to determine accurately by that method. It is possible to obtain k_2 from an analysis of the substrate concentration dependence of the rate of E·P complex formation (*35*, *36*). Toward this end, a plot of k_{obs} for E·P complex synthesis as a function of PAPS concentration was constructed (Figure 3). Rates were obtained from linear regression of averaged, duplicate four-point progress curves taken within the first 15% of E·P complex formation; further details are given in the legend of Figure 3. The data were fit using mechanism II, in which PAPS (or S) binding to $E \cdot E_2$ (or E) is at equilibrium. That PAPS binding is near equilibrium is consistent with the absence of a lag preceding the burst and is supported by the results of the isotope trapping experiment described below.

$$E + S \overset{k_{eq}}{\rightleftarrows} E \cdot S \overset{k_1}{\underset{k_2}{\rightleftarrows}} E \cdot P \qquad \text{(II)}$$

k_{obs} as a function of PAPS concentration for mechanism II is given by eq 3 (*35*, *36*):

$$k_{obs} = \frac{K_{eq} k_1 [PAPS]}{K_{eq}[PAPS] + 1} + k_2 \qquad (3)$$

which, when fit to the data, yields the following best-fit parameters: $K_{eq} = 4.0 \pm 0.3\ \mu M$, $k_1 = 3.4 \pm 0.1\ s^{-1}$, and $k_2 = 0.070 \pm 0.03\ s^{-1}$. The progress curve predicted by these parameters is represented by the solid line that passes through the data (Figure 3). Given these constants, one can calculate the equilibrium constant governing interconversion of the central complexes ($K_{eq\ int} \sim 49 = 3.4\ s^{-1}/0.07\ s^{-1}$).

Mechanism II assumes that all product (E·P) is capable of returning to ES, which is tantamount to assuming product is found entirely in ternary complex; alternatively, the concentrations of all complexes that cannot return to substrate (e.g., binary complexes) are treated as if they are negligible. If such nonreactive complexes comprise a substantial fraction of product, the model is in error, the concentration of ternary complex is diminished, and k_2 will increase to achieve the rate of ES formation needed to fit the k_{obs} versus [PAPS] data. That the majority of E·P is, in fact, in the ternary complex is supported by experiments discussed in the following section (Positioning the Rate-Determining Step).

A classical isotope trapping experiment (*37*, *38*) was performed to assess whether PAPS binding is near equilibrium during turnover. Briefly, EST (1.0 μM) was equilibrated at 25 °C with a saturating concentration of [^{35}S]PAPS (1.5 μM, K_d = 37 nM) and mixed rapidly with a solution of equal volume containing E_2 (3.6 μM, K_m = 5.0 nM) and a 1700-fold excess of unlabeled PAPS (2.7 mM). Experiments, performed in triplicate, revealed that under these conditions only 2.8 ± 0.2% of the enzyme-bound PAPS (assuming half-sites reactivity) was converted to product. Thus, the departure of PAPS from the enzyme is fast relative to its conversion to product, and PAPS binding is near equilibrium during turnover.

Positioning the Rate-Determining Step. While the burst reveals a rate-determining step(s) in the product release branch of the catalytic cycle, it does not identify which step(s) causes product to accumulate. If release of the first product from the ternary complex is fast relative to subsequent steps, then either a binary complex or E accumulates; notably, such complexes are incapable of returning to substrate. Alternatively, if release of the first product from the ternary complex is the slow step, the ternary complex accumulates, which, because of its full complement of ligands, can return to substrate. Thus, whether the enzyme-bound product that accumulates during the burst can form substrate is diagnostic of the type of complex and can be used to position the rate-determining step in the mechanism.

The extent to which the product complex can form substrate was assessed using an experiment that quantitates partitioning of this complex in the forward and reverse directions. A solution containing EST (1.0 μM) was mixed rapidly with an equal volume of a solution that was identical except that it lacked EST and contained E_2 (3.6 μM) and [^{35}S]PAPS (4.5 μM). The reaction was allowed to proceed for 0.30 s, at which point the burst is nearly complete and the enzyme-bound product forms are reaching their maximal concentration (see Figure 1). At 0.30 s, the solution was mixed a second time either with an equal volume of a chase solution containing a large excess (1022-fold) of unlabeled PAPS (2.3 mM) and E_2 (1.8 μM) or with a quench solution (NaOH, 0.66 M). The reactions for solutions mixed with chase were allowed to continue for 30 s prior to being quenched; during this 30 s interval, the radiolabeled reactants depart from the enzyme in the forward or reverse direction (as [^{35}S]E_2S or [^{35}S]PAPS, respectively). Departure is considered irreversible due either to vast dilution of labeled PAPS or to the fact that the

measurement is made at the very early stages of the forward reaction. The reactions (performed in triplicate) that were quenched immediately produced 0.44 ± 0.01 μM [^{35}S]E_2S (i.e., 88% of a half-site equivalent of EST), whereas those that were partitioned produced only 0.31 ± 0.02 μM [^{35}S]E_2S. Hence, partitioning reduced the yield of [^{35}S]E_2S by 30%, indicating that 30% of the E·PAP·[^{35}S]E_2S complex formed during the burst returns to substrate and departs from the enzyme as [^{35}S]PAPS.

Taken together, the 30% return of product to substrate complexes and the shape of the burst (zero intercept and monophasic) argue strongly that the majority of the product in the burst is in the ternary complex. The return of 30% of the labeled product to substrate confirms that at least this percentage of the product complexes is in the reactive ternary complex at the moment partitioning is initiated. If only 30% were in the ternary complex, all of it is trapped, and the remaining 70% is incapable of returning to substrate. In this case, the rate at which the ternary complex returns to substrate must be far greater than the rate at which it partitions forward to the other product forms found in the burst; were this not the case, the 30% would not have been trapped. Such a scenario predicts rapid equilibration of the substrate and product ternary complexes relative to the rate at which other products form and predicts a biphasic burst; the first phase reports on the equilibration of the ternary complexes and the second on decomposition of the ternary product complex to the other forms found in the burst. The burst shows no signs of multiple phases. It is well fit by a single phase with a zero intercept; thus, the majority of the product is in the ternary complex.

The Steady-State Balance of the Central Complexes Contributes to K_m. The K_d for PAPS binding to E·E_2 [4.0 μM (obtained by fitting k_{obs} vs [PAPS])] is far greater than the K_m for PAPS [59 nM (*3*)]. For mechanism III

$$E \underset{k_{off}}{\overset{[S]k_{on}}{\rightleftharpoons}} E{\cdot}S \underset{k_2}{\overset{k_1}{\rightleftharpoons}} E{\cdot}P \overset{k_3}{\rightarrow} E + P \qquad \text{(III)}$$

(which represents the binding of PAPS to E·E_2, followed by formation and release of product), K_m is given by eq 4.

$$K_m = \frac{k_{off}k_2 + k_{off}k_3 + k_1k_3}{k_{on}(k_1 + k_2 + k_3)} \qquad (4)$$

Applying the experimental constrains obtained from analysis of the burst ($k_1 \gg k_3$), k_{obs} versus [PAPS] ($k_1 \gg k_2$), and isotope trapping ($k_{off} \gg k_1$) results, we find eq 4 reduces to eq 5.

$$K_m = \frac{k_{off}}{k_{on}} \times \frac{k_2 + k_3}{k_1} \qquad (5)$$

Importantly, $(k_2 + k_3)/k_1$ represents the ratio of [E·S] to [E·P] in the steady state, $([E{\cdot}S]/[E{\cdot}P])_{ss}$. This can be seen by application of the steady-state assumption to the rate of formation and disappearance of EP:

$$\frac{dEP}{dt} = [ES]k_1 = [EP](k_2 + k_3) = -\frac{dEP}{dt} \qquad (6)$$

rearranging

$$\left(\frac{[ES]}{[EP]}\right)_{ss} = \frac{k_2 + k_3}{k_1} \qquad (7)$$

Thus, for the EST mechanism and other similar mechanisms (*39*), K_m is linked linearly to the steady-state mass ratio of the central complexes. Given values for k_1, k_2, and k_3 (4.4, 0.070, and 0.072 s^{-1}, respectively), we calculate $([E{\cdot}S]/[E{\cdot}P])_{ss}$ to be 0.031, which, when multiplied by K_d for PAPS binding to E·E_2, yields a K_m of 130 nM, a value that is in reasonable agreement with the published value of 59 nM.

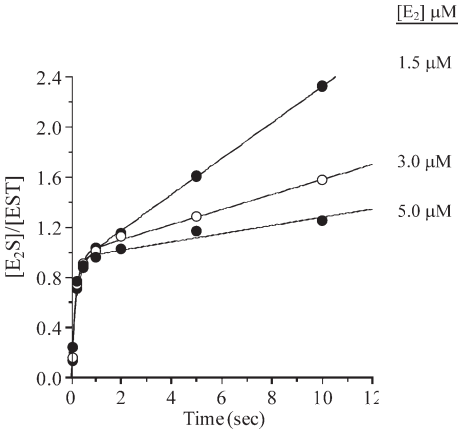

FIGURE 4: Effect of E_2 inhibition on the E_2S burst. We initiated the reactions by rapidly mixing a solution containing PAPS (18.0 μM), $MgCl_2$ (7.0 mM), DTT (1.0 mM), glycerol (10%, v/v), and 50 mM KPO_4 (pH 6.3) with an equal volume of an identical solution that did not contain PAPS but did contain EST (1.0 μM) and various concentrations of [^{3}H]E_2 (3.0, 6.0, and 10.0 μM). Quenching and product quantitation are described in the legend of Figure 1 (also, see Materials and Methods). Measurements were performed in triplicate and averaged. All solutions were equilibrated at 25 ± 2 °C prior to being mixed. Solid lines through the data represent the behavior predicted by the best-fit parameters obtained from a nonlinear least-squares fit of the parametrized form of eq 2 to the data (see Results and Discussion).

This analysis demonstrates that substrate affinity is enhanced ~30-fold through a selective balancing of rate constants to achieve a central complex mass ratio that favors product in the steady state. It is interesting to consider that changes in this ratio across a series of substrates will bias substrate selection. One cannot help but wonder which reactant features might interact with the enzyme to balance the central complexes and how alterations in such features might be used to control steady-state affinities and ultimately the metabolic disposition of a given sulfotransferase.

Substrate Inhibition Follows Chemistry. The forward reactions of sulfotransferases are typically inhibited by the non-nucleotidyl (or acceptor) substrate. In the case of EST, E_2 is a partial k_{cat} inhibitor [saturation with inhibitor decreases k_{cat} ~7-fold without altering $K_{m(PAPS)}$ (*3*)], and the inhibition constant [$K_{i(E2)}$ = 80 nM] is comparable to the levels of estrogen found in breast cystic fluid (*40*). The product burst provides an opportunity to fine-tune the point in the mechanism at which inhibition occurs. Toward this end, bursts were obtained at a series of inhibiting E_2 concentrations and compared. Remarkably, addition of E_2 to the inhibition pocket has no influence on the burst (Figure 4); thus, inhibition does not occur until the system reaches the product stages of the catalytic cycle. Notably, the E_2 concentrations needed to observe significant inhibition in the current experiments are higher than expected (*3*). This discrepancy is likely due to the very different conditions under which these measurements were taken. This finding is consistent with a variety of inhibition mechanisms. Previous work suggests that inhibition might occur via binding of E_2 at an allosteric site (*3*). While such a mechanism remains plausible, the burst

results are perhaps explained most simply by a model in which E_2 inhibits by binding to a form of the enzyme that appears only during the product stages; for example, the E·PAP complex, to which E_2 is known to bind (E·PAP·E_2), has been observed crystallographically (*41*), and interestingly, the structure gives no indication of an asymmetry that might lead to half-site reactivity. The dead-end inhibition mechanism predicts the onset of inhibition as E_2 binding to the E·PAP complex becomes fast with respect to release of PAP, thus trapping PAP in the dead-end complex. At an infinite E_2 concentration, one expects all of the E·PAP complex generated during turnover to be trapped in the E·PAP·E_2 complex and that further turnover requires that PAP "escape" directly from the dead-end complex. If PAP could not escape (for example, if release were strictly ordered with PAP releasing last), turnover would be driven to zero at an infinite E_2 concentration, and inhibition would be complete rather than partial. The fact that k_{cat} is non-zero when the E_2 concentration is extrapolated to infinity tells us that PAP does depart from the E·PAP·E_2 complex, and that its departure is rate-limiting at an infinite E_2 concentration; thus, k_{cat} extrapolated to an infinite E_2 concentration [i.e., 0.18 min^{-1} (*3*)] should provide an excellent approximation of the rate constant governing its departure from the E·PAP·E_2 complex.

CONCLUSIONS

Estrogen sulfotransferase exhibits half-sites reactivity. The mechanism of EST biases the central-complex equilibrium strongly toward product ($K_{eq\ int}$ = 49) and releases product slowly enough to allow the interconversion of the central complexes to approach equilibrium. Consequently, the steady-state ratio of the central complexes scales inversely with K_m and results in an ~30-fold increase in the affinity of EST for its substrates. Thus, the steady-state affinity of the enzyme for substrate is determined by a balance of kinetic factors that begin at the point of binding and reach as far into the mechanism as interactions with the product central complexes. It will be interesting to explore whether such factors contribute to substrate selectivity in the sulfotransferase family.

Consistent with formation of an E·PAPS·E_2 dead-end complex, inhibition of EST by E_2 occurs after formation of the product central complex. Assuming the dead-end mechanism, one is led to conclude that departure of PAP from the E·PAP·E_2 complex is rate-determining in the inhibited system and that k_{cat} extrapolated to an infinite E_2 concentration (0.18 min^{-1}) approximates the PAP release rate constant.

The findings of this work have shed new light on the mechanism of EST (and presumably other members of the sulfotransferase family) and raise intriguing questions regarding the molecular basis of half-sites reactivity in this system and the catalytic and biological necessity for such a mechanism in regulating estrogen metabolism and sulfuryl transfer in general.

REFERENCES

1. Leyh, T. S. (1993) The physical biochemistry and molecular genetics of sulfate activation. *Crit. Rev. Biochem. Mol. Biol. 28*, 515–542.
2. Robbins, P. W., and Lipmann, F. (1958) Enzymatic synthesis of adenosine-5′-phosphosulfate. *J. Biol. Chem. 233*, 686–690.
3. Zhang, H., Varlamova, O., Vargas, F. M., Falany, C. N., and Leyh, T. S. (1998) Sulfuryl transfer: The catalytic mechanism of human estrogen sulfotransferase. *J. Biol. Chem. 273*, 10888–10892.
4. Lu, L. Y., Chiang, H. P., Chen, W. T., and Yang, Y. S. (2009) Dimerization is responsible for the structural stability of human sulfotransferase 1A1. *Drug Metab. Dispos. 37*, 1083–1088.
5. Petrotchenko, E. V., Pedersen, L. C., Borchers, C. H., Tomer, K. B., and Negishi, M. (2001) The dimerization motif of cytosolic sulfotransferases. *FEBS Lett. 490*, 39–43.
6. Weitzner, B., Meehan, T., Xu, Q., and Dunbrack, R. L., Jr. (2009) An unusually small dimer interface is observed in all available crystal structures of cytosolic sulfotransferases. *Proteins 75*, 289–295.
7. Hahnel, R., Twaddle, E., and Ratajczak, T. (1973) The specificity of the estrogen receptor of human uterus. *J. Steroid Biochem. 4*, 21–31.
8. Ghosh, D. (2007) Human sulfatases: aA structural perspective to catalysis. *Cell. Mol. Life Sci. 64*, 2013–2022.
9. Iwamori, M. (2005) Estrogen sulfatase. *Methods Enzymol. 400*, 293–302.
10. Falany, C. N., Wheeler, J., Oh, T. S., and Falany, J. L. (1994) Steroid sulfation by expressed human cytosolic sulfotransferases. *J. Steroid Biochem. Mol. Biol. 48*, 369–375.
11. Pasqualini, J. R., Schatz, B., Varin, C., and Nguyen, B. L. (1992) Recent data on estrogen sulfatases and sulfotransferases activities in human breast cancer. *J. Steroid Biochem. Mol. Biol. 41*, 323–329.
12. Brand, S. J., Andersen, B. N., and Rehfeld, J. F. (1984) Complete tyrosine-O-sulphation of gastrin in neonatal rat pancreas. *Nature 309*, 456–458.
13. Jen, C. H., Moore, K. L., and Leary, J. A. (2009) Pattern and temporal sequence of sulfation of CCR5 N-terminal peptides by tyrosylprotein sulfotransferase-2: An assessment of the effects of N-terminal residues. *Biochemistry 48*, 5332–5338.
14. Lee, S. W., Han, S. W., Sririyanum, M., Park, C. J., Seo, Y. S., and Ronald, P. C. (2009) A type I-secreted, sulfated peptide triggers XA21-mediated innate immunity. *Science 326*, 850–853.
15. Roth, J. A., and Rivett, A. J. (1982) Does sulfate conjugation contribute to the metabolic inactivation of catecholamines in humans? *Biochem. Pharmacol. 31*, 3017–3021.
16. Hassan, H. H. (2007) Chemistry and biology of heparin mimetics that bind to fibroblast growth factors. *Mini Rev. Med. Chem. 7*, 1206–1235.
17. Lindahl, U. (2007) Heparan sulfate-protein interactions: A concept for drug design? *Thromb. Haemostasis 98*, 109–115.
18. Atha, D. H., Lormeau, J. C., Petitou, M., Rosenberg, R. D., and Choay, J. (1985) Contribution of monosaccharide residues in heparin binding to antithrombin III. *Biochemistry 24*, 6723–6729.
19. Leyte, A., van Schijndel, H. B., Niehrs, C., Huttner, W. B., Verbeet, M. P., Mertens, K., and van Mourik, J. A. (1991) Sulfation of Tyr1680 of human blood coagulation factor VIII is essential for the interaction of factor VIII with von Willebrand factor. *J. Biol. Chem. 266*, 740–746.
20. Stone, S. R., and Hofsteenge, J. (1986) Kinetics of the inhibition of thrombin by hirudin. *Biochemistry 25*, 4622–4628.
21. Hortin, G. L., Farries, T. C., Graham, J. P., and Atkinson, J. P. (1989) Sulfation of tyrosine residues increases activity of the fourth component of complement. *Proc. Natl. Acad. Sci. U.S.A. 86*, 1338–1342.
22. Glatt, H. (2000) Sulfotransferases in the bioactivation of xenobiotics. *Chem.-Biol. Interact. 129*, 141–170.
23. Kauffman, F. C. (2004) Sulfonation in pharmacology and toxicology. *Drug Metab. Rev. 36*, 823–843.
24. Coughtrie, M. W. (2002) Sulfation through the looking glass: Recent advances in sulfotransferase research for the curious. *Pharmacogenomics J. 2*, 297–308.
25. Weinshilboum, R. M., Otterness, D. M., Aksoy, I. A., Wood, T. C., Her, C., and Raftogianis, R. B. (1997) Sulfation and sulfotransferases 1: Sulfotransferase molecular biology: cDNAs and genes. *FASEB J. 11*, 3–14.
26. Glatt, H., and Meinl, W. (2004) Pharmacogenetics of soluble sulfotransferases (SULTs). *Naunyn-Schmiedeberg's Arch. Pharmacol. 369*, 55–68.
27. Falany, J. L., and Falany, C. N. (1996) Expression of cytosolic sulfotransferases in normal mammary epithelial cells and breast cancer cell lines. *Cancer Res. 56*, 1551–1555.
28. Falany, J. L., and Falany, C. N. (1997) Regulation of estrogen activity by sulfation in human MCF-7 breast cancer cells. *Oncol. Res. 9*, 589–596.
29. Qian, Y., Deng, C., and Song, W. C. (1998) Expression of estrogen sulfotransferase in MCF-7 cells by cDNA transfection suppresses the estrogen response: Potential role of the enzyme in regulating estrogen-dependent growth of breast epithelial cells. *J. Pharmacol. Exp. Ther. 286*, 555–560.
30. Gill, S. C., and von Hippel, P. H. (1989) Calculation of protein extinction coefficients from amino acid sequence data. *Anal. Biochem. 182*, 319–326.
31. Sun, M., and Leyh, T. S. (2006) Channeling in sulfate activating complexes. *Biochemistry 45*, 11304–11311.

32. Liu, C., Martin, E., and Leyh, T. S. (1994) GTPase activation of ATP sulfurylase: The mechanism. *Biochemistry 33*, 2042–2047.
33. Mendes, P. (1997) Biochemistry by numbers: Simulation of biochemical pathways with Gepasi 3. *Trends Biochem. Sci. 22*, 361–363.
34. Wei, J., Tang, Q. X., Varlamova, O., Roche, C., Lee, R., and Leyh, T. S. (2002) Cysteine biosynthetic enzymes are the pieces of a metabolic energy pump. *Biochemistry 41*, 8493–8498.
35. Johnson, K. A. (1986) Rapid kinetic analysis of mechanochemical adenosinetriphosphatases. *Methods Enzymol. 134*, 677–705.
36. Johnson, K. A. (1992) Transient-state kinetic analysis of enzyme reaction pathways. *Enzymes XX*, 1–61.
37. Cleland, W. W. (1975) Partition analysis and the concept of net rate constants as tools in enzyme kinetics. *Biochemistry 14*, 3220–3224.
38. Rose, I. A. (1980) The isotope trapping method: Desorption rates of productive E·S complexes. *Methods Enzymol. 64*, 47–59.
39. Lieser, S. A., Aubol, B. E., Wong, L., Jennings, P. A., and Adams, J. A. (2005) Coupling phosphoryl transfer and substrate interactions in protein kinases. *Biochim. Biophys. Acta 1754*, 191–199.
40. Pasqualini, J. R., Gelly, C., Nguyen, B. L., and Vella, C. (1989) Importance of estrogen sulfates in breast cancer. *J. Steroid Biochem. 34*, 155–163.
41. Kakuta, Y., Pedersen, L. G., Carter, C. W., Negishi, M., and Pedersen, L. C. (1997) Crystal structure of estrogen sulphotransferase. *Nat. Struct. Biol. 4*, 904–908.